Econ. Environ. Geol.
Vol. 30, No. 5, p. 433-442, 1997.

Dual-permeability Fractal Model of Groundwater Flow in Fissured Aquifers

Pascal Bidaux* and Se-Yeong Hamm**

ABSTRACT : A dual-permeability fractal model of fluid flow is proposed. The model simulates groundwater flow in fissured dual aquifer system composed of Aquifer 1 and Aquifer 2. For this model, groundwater flow originates only from Aquifer 1 on the pumping well. The model considers wellbore storage and skin effects at the pumping well and then shows exact drawdown at the early time of pumping. Type curves for different flow dimensions and for two cases are presented and analyzed. The case 1 represents the aquifer system which consists of Aquifer 1 with low permeability and high specific storage and Aquifer 2 with high permeability and low specific storage. The case 2 is inverse to the case 1. Dimensionless drawdown curves in Aquifer 1 and Aquifer 2 shows characteristic trend each other. Consequently, the model will be useful to analyze pumping test data of different drawdown patterns on the pumping well and observation wells.

INTRODUCTION

Several theories of groundwater flow in fractured rocks have been developed since 1960's (Barenblatt *et al.*, 1960; Warren, Root, 1963; Kazemi, 1969; Boulton, Streltsova, 1977; Jenkins, Prentice, 1982; Cinco-Ley, Samaniego-V., 1981). All the models mentioned above are based on a Cartesian description of the reservoir and hence integral flow dimensions. So, all of them can not treat exactly physical properties of flow in fractured rocks because of their limitation to integral flow dimensions.

It is recognized that flow in fissured rocks is controlled by the fissure network which often has a fractal geometry (Allègre *et al.*, 1982; Thomas, 1987; Velde *et al.*, 1991). The principal idea of fractal theory is that a phenomenon may be repeated in the same way at different scales. Consequently, the measure of this phenomenon increases as a non-integral power of scale. Groundwater flow analysis by fractal theory has been introduced by Barker (1988) and Chang, Yortsos (1988), who defined the concept of non-integral flow dimension. Hamm, Bidaux (1994a) proposed a fractal theory with leakage from aquitard, that generalize Hantush's equation (1956). Hamm, Bidaux (1994b) also proposed the dual-porosity fractal model of steady-state flow which generalizes Warren-Root model (1963). Acuna, Yortsos (1995) applied fractal networks of fractures for numerical simulation of unsteady single-phase flow. Hamm, Bidaux (1996) proposed dual-porosity fractal model of transient flow in fractured media with fracture skin between fissures and matrix blocks and their relation with steady-state dual-porosity fractal model.

Limitations in these fractal models appear when drawdown response is much different between on the pumping well and on the observation well. The phenomenon indicates the flow system of several fracture sub-networks (that is, several fractured media) having distinct hydraulic properties. Hence, we propose a dual-permeability model of fluid flow in two superposed fractured aquifers (Aquifer 1 and Aquifer 2). As a consequence of a hierarchy in fracture apertures, hydraulic connections between the fractured media may be limited. Narrow fissures that link the fractured aquifers would play a role that is somewhat similar to that of semi-pervious layers. Hence, except for the fractal geometry, such a reservoir may behave like a multi-layered system in Euclidean geometry. The model considers wellbore storage and skin effects at the pumped well, and can be easily utilized for the multi-well and multi-rate pumping system composed of several pumping and observation wells.

THEORY

The main assumptions of the model is as follows:

Flow is radial, n-dimensional and it converges towards a single source of radius r_w, pumped at a constant rate Q.

* Perenco 21 av. Victor Hugo, 75116 Paris, France
** 부산대학교 지질학과 (Pusan National University, Pusan 609-735, Korea)

The reservoir consists of two overlapping, confined, homogeneous and isotropic fractured media of infinite extent in the radial direction which are referred as Aquifer 1 (the lower aquifer) and Aquifer 2 (the upper aquifer). Within Aquifer 1 and Aquifer 2, fluid flow obeys Darcy's law and fluid storage is elastic. Aquifer i is characterized by a hydraulic conductivity K_i, specific storage S_{si}, and transverse extent b_i. At any radial distance r from the source and at any time t, drawdown s_1 in Aquifer 1 and s_2 in Aquifer 2 may be different.

The source only penetrates Aquifer 1. It is characterized by a wellbore storage constant W_s and skin factor s_f. Darcy's law is applied to the exchange of fluid between Aquifer 1 and the source.

Darcy's law is applied to the exchange of fluid by formation crossflow between Aquifer 1 and Aquifer 2. Formation crossflow is characterized by the interface semi-permeability coefficient, χ.

Any piezometers indicate the local drawdown in either Aquifer 1 or Aquifer 2, but do not induce hydraulic short circuits between both aquifers.

Following Barker (1988), let us express the volumes of fluid ΔV_1 and ΔV_2, released by Aquifer 1 and Aquifer 2, respectively, during a small period Δt, in the region between the equipotential surfaces which have radii r and r+Δr, where Δr is small:

$$\Delta V_1 = S_{S1} b_1^{3-n} \alpha_n r^{n-1} \Delta r \Delta s_1 \tag{1}$$

$$\Delta V_2 = S_{S2} b_2^{3-n} \alpha_n r^{n-1} \Delta r \Delta_2 \tag{2}$$

in which Δs_1 and Δs_2 denote the drawdown change in Aquifer 1 and Aquifer 2, respectively; and α_n is the area of a unit sphere in n dimensions and is expressed as:

$$\alpha_n = 2\pi^{n/2} / \Gamma(n/2) \tag{3}$$

where $\Gamma(x)$ is the Gamma function.

The net volumetric flow rates out from the shell, for Aquifer 1 and Aquifer 2, respectively, are expressed as

$$q_1 = K_1 b_1^{3-n} \alpha_n \left[(r+\Delta r)^{n-1} \frac{\partial s_1}{\partial r}(r+\Delta r,\ t) - r^{n-1} \frac{\partial s_1}{\partial r}(r,t) \right] \tag{4}$$

$$q_2 = K_2 b_2^{3-n} \alpha_n \left[(r+\Delta r)^{n-1} \frac{\partial s_2}{\partial r}(r+\Delta r,\ t) - r^{n-1} \frac{\partial s_2}{\partial r}(r,\ t) \right] \tag{5}$$

From Darcy's law, the algebraic crossflow rate q_χ from Aquifer 1 to Aquifer 2, inside the shell, is proportional to χ ($L^{2-n}T^{-1}$), to the contact area at the interface between Aquifer 1 and Aquifer 2, and to the local difference between drawdowns in Aquifer 1 and Aquifer 2. It is given by

$$q_\chi = \chi(\alpha_n r^{n-1} \Delta r)(s_1 - s_2) \tag{6}$$

Fluid conservation equations for Aquifer 1 and Aquifer 2 in the shell are:

$$\Delta V_1 = (q_1 - q_\chi)\Delta t \tag{7}$$

$$\Delta V_2 = (q_2 + q_\chi)\Delta t \tag{8}$$

from which the frow equations in the reservoir are obtained by taking limits:

$$S_{s1} b_1^{3-n} \frac{\partial s_1}{\partial t} = K_1 \frac{b_1^{3-n}}{r^{n-1}} \frac{\partial}{\partial r} \left(r^{n-1} \frac{\partial s_1}{\partial r} \right) + \chi(s_2 - s_1) \tag{9}$$

$$S_{s2} b_2^{3-n} \frac{\partial s_2}{\partial t} = \frac{K_2 b_2^{3-n}}{r^{n-1}} \frac{\partial}{\partial r} \left(r^{n-1} \frac{\partial s_2}{\partial r} \right) + \chi(s_1 - s_2) \tag{10}$$

The existence of formation crossflow induces a linear coupling between flow equations in Aquifer 1 and Aquifer 2. Hence, equations (9) and (10) cannot be solved separately.

Let s_w be the drawdown at the source. As the source only penetrates Aquifer 1, we have:

$$W_s \frac{\partial s_w}{\partial t} = Q + K_f b^{3-n} \alpha_n r_w^{n-1} \left(\frac{\partial s_1}{\partial r} \right)_{r=r_w} \tag{11}$$

in which W_s is the wellbore storage constant of the source; i. e., the volume of fluid stored or released for unit change of drawdown. We also have a singular head loss at the entry of the source; by definition of the skin factor:

$$s_w(t) = s_1(r_w,\ t) - s_f r_w \left(\frac{\partial s_1}{\partial r} \right)_{r=r_w} \tag{12}$$

Aquifer 2 is not penetrated by the source; hence, r = r_w behaves like a no-flow boundary for Aquifer 2:

$$\left(\frac{\partial s_2}{\partial r} \right)_{r=r_w} = 0 \tag{13}$$

The system is initially at rest:

$$s_w(r, 0) = s_1(r, 0) = s_2(r, 0) = 0 \tag{14}$$

In addition, the reservoir has an infinite radial extent:

$$s_1(\infty, t) = s_2(\infty, t) = 0 \tag{15}$$

Let us define the following dimensionless variables:

$$t_D = \frac{4(K_1 b_1^{3-n} + K_2 b_2^{3-n})}{r_w^2(S_{s1} b_1^{3-n} + S_{s2} b_2^{3-n})} t \tag{16}$$

$$r_D = r/r_w \tag{17}$$

$$s_{iD} = \frac{4\pi^{n/2}(K_1 b_1^{3-n} + K_2 b_2^{3-n})}{Q r_w^{2-n}} s_i$$

$$(i = 1 \text{ (Aquifer 1)}, 2 \text{ (Aquifer 2)}, w) \tag{18}$$

$$W_{sD} = \frac{W_s}{\pi^{n/2} r_w^n (S_{s1} b_1^{3-n} + S_{s2} b_2^{3-n})} \tag{19}$$

$$\omega = \frac{S_{s1} b_1^{3-n}}{S_{s1} b_1^{3-n} + S_{s2} b_2^{3-n}} \tag{20}$$

$$\kappa = \frac{K_1 b_1^{3-n}}{K_1 b_1^{3-n} + K_2 b_2^{3-n}} \tag{21}$$

$$\lambda = \frac{\chi r_w^2}{K_1 b_1^{3-n} + K_2 b_2^{3-n}} \tag{22}$$

Equations (9) through (13) become:

$$\frac{\kappa}{r_D^{n-1}} \frac{\partial}{\partial r_D} \left(r_D^{n-1} \frac{\partial s_{1D}}{\partial r_D} \right) = 4\omega \frac{\partial s_{1D}}{\partial t_D} + \lambda(s_{1D} - s_{2D}) \tag{23}$$

$$\frac{1-\kappa}{r_D^{n-1}} \frac{\partial}{\partial r_D} \left(r_D^{n-1} \frac{\partial s_{2D}}{\partial r_D} \right) = 4(1-\omega) \frac{\partial s_{2D}}{\partial t_D} + \lambda\left(s_{2D} - s_{1D}\right) \tag{24}$$

$$W_{sD} \frac{\partial s_{wD}}{\partial t_D} = 1 + \frac{\kappa}{2\Gamma(n/2)} \left(\frac{\partial s_{1D}}{\partial r_D} \right)_{r_D = 1} \tag{25}$$

$$s_{wD}(t_D) = s_{1D}(1, t_D) - s_f \left(\frac{\partial s_{1D}}{\partial r_D} \right)_{r_D = 1} \tag{26}$$

$$\left(\frac{\partial s_{2D}}{\partial r_D} \right)_{r_D = 1} = 0 \tag{27}$$

Applying dimensionless Laplace transform to those equations, we obtain:

$$\frac{\kappa}{r_D^{n-1}} \frac{d}{dr_D} \left(r_D^{n-1} \frac{d\bar{s}_{1D}}{dr_D} \right) = 4\omega p \bar{s}_{1D} + \lambda(\bar{s}_{1D} - \bar{s}_{2D}) \tag{28}$$

$$\frac{1-\kappa}{r_D^{n-1}} \frac{d}{dr_D} \left(r_D^{n-1} \frac{d\bar{s}_{2D}}{dr_D} \right) = 4(1-\omega) p \bar{s}_{2D} + \lambda(\bar{s}_{2D} - \bar{s}_{1D}) \tag{29}$$

$$p W_{sD} \bar{s}_{wD} = \frac{1}{p} + \frac{\kappa}{2\Gamma(n/2)} \left(\frac{d\bar{s}_{1D}}{dr_D} \right)_{r_D = 1} \tag{30}$$

$$\bar{s}_{wD}(p) = \bar{s}_{1D}(1, p) - s_f \left(\frac{d\bar{s}_{1D}}{dr_D} \right)_{r_D = 1} \tag{31}$$

$$\left(\frac{d\bar{s}_{2D}}{dr_D} \right)_{r_D = 1} = 0 \tag{32}$$

in which p is Laplace variable. We now try to find auxiliary variables which would allow a de-coupling of Eqs. (28) and (29). Those can be rearranged as

$$\frac{\sqrt{\kappa}}{r_D^{n-1}} \frac{d}{dr_D} \left(r_D^{n-1} \frac{d(\sqrt{\kappa}\,\bar{s}_{1D})}{dr_D} \right) = \frac{4\omega p + \lambda}{\sqrt{\kappa}} (\sqrt{\kappa}\,\bar{s}_{1D}) - \frac{\lambda}{\sqrt{1-\kappa}} (\sqrt{1-\kappa}\,\bar{s}_{2D}) \tag{33}$$

$$\frac{\sqrt{1-\kappa}}{r_D^{n-1}} \frac{d}{dr_D} \left(r_D^{n-1} \frac{d(\sqrt{1-\kappa}\,\bar{s}_{2D})}{dr_D} \right) = \frac{4(1-\omega)p + \lambda}{\sqrt{1-\kappa}} (\sqrt{1-\kappa}\,\bar{s}_{2D}) - \frac{\lambda}{\sqrt{\kappa}} (\sqrt{\kappa}\,\bar{s}_{1D}) \tag{34}$$

The differential system above can be written in matrix from:

$$\frac{1}{r_D^{n-1}} \frac{d}{dr_D} \left(r_D^{n-1} \frac{dX}{dr_D} \right) = W \cdot X \tag{35}$$

with

$$X = \frac{\sqrt{\kappa}\,\bar{s}_{1D}}{\sqrt{1-\kappa}\,\bar{s}_{2D}} \tag{36}$$

and

$$W = \begin{bmatrix} \frac{4\omega p + \lambda}{\kappa} & -\frac{\lambda}{\sqrt{\kappa(1-\kappa)}} \\ -\frac{\lambda}{\sqrt{\kappa(1-\kappa)}} & \frac{4(1-\omega)p + \lambda}{1-\kappa} \end{bmatrix} \tag{37}$$

For any value of p, the matrix W is symmetric, definite, positive. Hence, it is possible to diagonalize W: i, e., to find an orthogonal matrix (a rotation) :

$$R_\theta = \begin{pmatrix} \cos\theta & -\sin\theta \\ \sin\theta & \cos\theta \end{pmatrix} \tag{38}$$

and a diagonal matrix with strictly positive coefficients:

$$\sum^2 = \begin{pmatrix} \sigma_1^2 & 0 \\ 0 & \sigma_2^2 \end{pmatrix} \tag{39}$$

such that

$$W = R_{-\theta} \cdot \sum^2 \cdot R_\theta \tag{40}$$

Substituting (40) to (35) makes:

$$\frac{1}{r_D^{n-1}} \frac{d}{dr_D}\left(r_D^{n-1} \frac{dX}{dr_D} \right) = R_{-\theta} \cdot \sum^2 \cdot R_\theta \cdot X \tag{41}$$

Multiplying both sides by R_θ, we obtain:

$$\frac{1}{r_D^{n-1}} \frac{d}{dr_D}\left(r_D^{n-1} \frac{dX}{dr_D} \right) = \sum^2 \cdot U \tag{42}$$

in which we have defined

$$U = \begin{pmatrix} u_1 \\ u_2 \end{pmatrix} = R_\theta \cdot X = \begin{pmatrix} \sqrt{\kappa}\,\bar{s}_{1D}\cos\theta - \sqrt{1-\kappa}\,\bar{s}_{2D}\sin\theta \\ \sqrt{\kappa}\,\bar{s}_{1D}\sin\theta + \sqrt{1-\kappa}\,\bar{s}_{2D}\cos\theta \end{pmatrix} \tag{43}$$

Eqs. (28) and (29) have finally been replaced by the following equivalent de-coupled form :

$$\frac{1}{r_D^{n-1}} \frac{d}{dr_D}\left(r_D^{n-1} \frac{du_1}{dr_D} \right) = \sigma_1^2 \cdot u_1 \tag{44}$$

$$\frac{1}{r_D^{n-1}} \frac{d}{dr_D}\left(r_D^{n-1} \frac{du_2}{dr_D} \right) = \sigma_2^2 \cdot u_2 \tag{45}$$

by using the new independent variables u_1 and u_2. Those obey equations who have the same form that the equation governing hydraulic head distribution in Laplace domain for Barker's model. Hence, the general solution for u_1 and u_2 is:

$$u_1 = A_1 r_D^{\nu} K_\nu(\sigma_1 r_D) \tag{46}$$

$$u_2 = A_2 r_D^{\nu} K_\nu(\sigma_2 r_D) \tag{47}$$

in which

$$\nu = 1 - n/2 \tag{48}$$

and $K_\nu(\mu)$ is modified Bessel function of second kind and order ν.

Inverting (43) to express $\bar{s}_{1D}$ and $\bar{s}_{2D}$ as functions of u_1 and u_2, and substituting from (46) and (47), we obtain the general solution for the dimensionless drawdowns in Aquifer 1 and Aquifer 2 :

$$\bar{s}_{1D} = \frac{A_1 r_D^{\nu} K_\nu(\sigma_1 r_D)\cos\theta + A_2 r_D^{\nu} K_\nu(\sigma_2 r_D)\sin\theta}{\sqrt{\kappa}} \tag{49}$$

$$\bar{s}_{2D} = \frac{-A_1 r_D^{\nu} K_\nu(\sigma_1 r_D)\sin\theta + A_2 r_D^{\nu} K_\nu(\sigma_2 r_D)\cos\theta}{\sqrt{1-\kappa}} \tag{50}$$

Taking the derivatives of (49) and (50), and (52), the values of the source (r_D=1) are obtained:

$$\left(\frac{\partial \bar{s}_{1D}}{\partial r_D} \right)_{r_D = 1} = \frac{-A_1\sigma_1 K_{\nu-1}(\sigma_1)\cos\theta - A_2\sigma_2 K_{\nu-1}(\sigma_2)\sin\theta}{\sqrt{\kappa}} \tag{51}$$

$$\left(\frac{\partial \bar{s}_{2D}}{\partial r_D} \right)_{r_D = 1} = \frac{A_1\sigma_1 K_{\nu-1}(\sigma_1)\sin\theta - A_2\sigma_2 K_{\nu-1}(\sigma_2)\cos\theta}{\sqrt{1-\kappa}} \tag{52}$$

Using (49), (51) and (52), equations (30), (31), and (32) can be written as

$$pW_{sD}\bar{s}_{wD} = \frac{1}{p} - \frac{\sqrt{\kappa}}{2\Gamma(n/2)} [A_1\sigma_1 K_{\nu-1}(\sigma_1)\cos\theta + A_2\sigma_2 K_{\nu-1}(\sigma_2)\sin\theta] \tag{53}$$

$$s_{wD} = \frac{[A_1 K_\nu(\sigma_1)\cos\theta + A_2 K_\nu(\sigma_2)\sin\theta]}{\sqrt{\kappa}} +$$

$$\frac{s_f[A_1(\sigma_1)K_{\nu-1}\cos\theta+A_2\sigma_2K_{\nu-1}(\sigma_2)\sin\theta]}{\sqrt{\kappa}} \quad (54)$$

$$A_1\sigma_1K_{\nu-1}(\sigma_1)\sin\theta-A_2\sigma_2K_{\nu-1}(\sigma_2)\cos\theta=0 \quad (55)$$

which is , for any value of p, a regular linear system with 3 equations and 3 unknown : $\bar{s}_{wD}$ and the two integration constants, A_1 and A_2. Solving this system gives the solution for dimensionless drawdown at the pumping well in Laplace domain :

$$\bar{s}_{wD}=\frac{1}{p}\left(pW_{sD}+\frac{\kappa}{2\Gamma(n/2)}\frac{1}{K^{\nu}_{\nu-1}(\sigma_1)\cos^2\theta+K^{\nu}_{\nu-1}(\sigma^2)\sin^2\theta+s_f}\right) \quad (56)$$

where $K^{\nu}_{\nu-1}(z)=K_{\nu}(z)/(zK_{\nu-1}(z))$

For piezometers, rather than taking the full expression of A_1 and A_2, we eliminate $\bar{s}_{wD}$ from (53) by setting wellbore storage to zero, and we solve the simplified system ((53) and (55)) for A_1 and A_2. Substituting their values in (49) and (50) and rearranging (49) and (50), we finally get dimensionless drawdowns, in Laplace domain, at an observation well in Aquifer 1 and Aquifer 2, $\bar{s}_{1D}$ and $\bar{s}_{2D}$, respectively :

$$\bar{s}_{1D}=\frac{2^{1+\nu}r_D^{\nu}}{p\kappa}\left[\frac{K_{\nu}(\sigma_1r_D)\cos^2\theta}{\sigma_1^{\nu}}+\frac{K_{\nu}(\sigma_2r_D)\sin^2\theta}{\sigma_2^{\nu}}\right] \quad (57)$$

$$\bar{s}_{2D}=\frac{2^{1+\nu}r_D^{\nu}\sin\theta\cos\theta}{p\sqrt{\kappa(1-\kappa)}}\left[\frac{K_{\nu}(\sigma_2r_D)}{\sigma_2^{\nu}}-\frac{K_{\nu}(\sigma_1r_D)}{\sigma_1^{\nu}}\right] \quad (58)$$

where,

$$\sigma_1=\left[\frac{m_1+m_2+(m_1-m_2)\sqrt{1+t^2}}{2}\right]^{1/2} \quad (59)$$

$$\sigma_2=\left[\frac{m_1+m_2-(m_1-m_2)\sqrt{1+t^2}}{2}\right]^{1/2} \quad (60)$$

$$\cos\theta=\left[\frac{\sqrt{1+t^2}+1}{2\sqrt{1+t^2}}\right]^{1/2} \quad (61)$$

$$\sin\theta=\left[\frac{\sqrt{1+t^2}-1}{2\sqrt{1+t^2}}\right]^{1/2} \quad (62)$$

$$t=\frac{2n}{m_1-m_2} \quad (63)$$

$$m_1=\frac{4\omega p+\lambda}{\kappa} \quad (64)$$

$$m_1=\frac{4(1-\omega p)+\lambda}{1-\kappa} \quad (65)$$

$$n=\frac{\lambda}{\sqrt{\kappa(1-\kappa)}} \quad (66)$$

In order to compute drawdowns as a function of time in the general case, we used a pakage developed by Amos (1986) to evaluate modified Bessel functions and Stehfest algorithm (1970) to invert Laplace transforms.

TYPE CURVES

We plotted several type curves for two cases: the case 1 (K_1/S_{s1}=2 m^2s^{-1}, K_2/S_{s2}=0.002 m^2s^{-1} and S_{s2}/S_{s1}= 10) and the case 2 (K_1/S_{s1}=0.002 m^2s^{-1}, K_2/S_{s2}=2 m^2s^{-1} and S_{s2}/S_{s1}=0.1). Fig. 1 and Fig. 2 present the case 1, and Fig. 3 and Fig. 4 present the case 2. Fig. 1 (a) to (f) show logarithmic dimensionless drawdown (s_{wD}) versus logarithmic dimensionless time(t_D/r_D^2) of, respectively, n = 0.5, 1, 1.5, 2, 2.5 and 3 at the pumping well. Similar to dual-porosity fractal model of steady-state flow (Hamm, Bidaux, 1994b), one can distinguish three parts of the curves except flow dimensions above 2. The first part of the curves shows the effect of wellbore storage followed by influence of flow in Aquifer 1. The second part (the transition zone) shows progressive contribution from Aquifer 2. Finally, The third part shows the behavior of homogenous combination of Aquifer 1 and Aquifer 2. If the value of λ is large, the second part begins before disappearance of wellbore storage effect. Contrarily, when the value of λ is small, the second part begins much late. In that case, one risks to confuse the fractal model of dual-permeability with Baker's model. Any type curves of greater than flow dimension 2 appear almost the same regardlessly the values of λ, stabilizing next to the wellbore storage effect.

Solid lines of Fig. 2(a) to (f) show logarithmic dimensionless drawdown (s_{1D}/r_D^{2-n}) versus logarithmic dimensionless time(t_D/r_D^2) of, respectively, n=0.5, 1, 1.5, 2, 2.5 and 3 at an observation well in Aquifer 1 for case 1. For the case of Aquifer 1, similar to dual-porosity fractal model of steady-state flow (Hamm, Bidaux, 1994b), one can distinguish three parts of the curves: the first part of the curves presents flow from Aquifer 1; the second part (the transition zone) shows progressive contribution from Aquifer 2; the third part shows the behavior of homogenous total system of

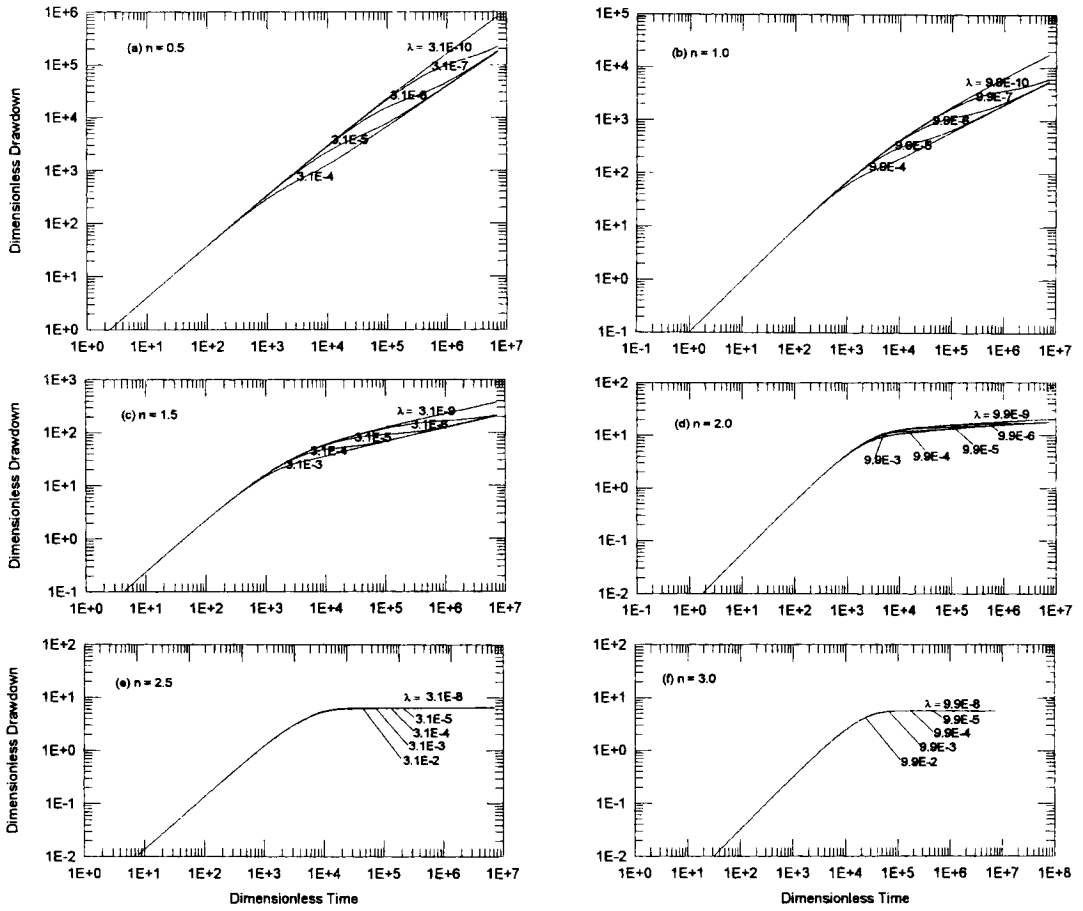

Fig. 1. Dimensionless drawdown curves at the production well in Aquifer 1 with different values of λ and various flow dimensions (W_S=0.03, S_F=0, κ=0.99 and ω=0.091).

both Aquifer 1 and Aquifer 2. The larger the value of λ, the smaller the drawdown.

Broken lines of Fig. 2 (a) to (f) show logarithmic dimensionless drawdown (s_{2D}/r_D^{2-n}) versus logarithmic dimensionless time(t_D/r_D^2) of, respectively, n=0.5, 1, 1.5, 2, 2.5 and 3 at an observation well in Aquifer 2. One can divide three parts on the lines: the first part nearly shows straight line; the second part (the transition zone) less distinctive than that of Aquifer 1 and does not show the stabilization; the third part shows the behavior of homogenous total system of both Aquifer 1 and Aquifer 2 and the curves of Aquifer 1 and Aquifer 2 join together. Contrarily to the case of the observation well in Aquifer 1, the smaller the value of λ, the smaller the drawdown. As the value of λ is large, the curve follows the behavior of homogenous total system fast. For the same values of λ, the drawdown is becoming smaller with increasing the flow dimension.

Fig. 3 (a) to (f) show logarithmic dimensionless drawdown (s_{wD}) versus logarithmic dimensionless time(t_D/r_D^2) of, respectively, n=0.5, 1, 1.5, 2, 2.5 and 3 at the pumping well for case 2. In almost all of flow dimensions except dimension 1, one can only distinguish two parts of the curves because of long period of transition zone. The first part of the curves shows the effect of wellbore storage followed by influence of flow in Aquifer 1. The second part (the transition zone) shows important contribution from Aquifer 2 with stabilization. The larger the value of λ, the smaller the drawdown.

Solid lines of Fig. 4(a) to (f) illustrate logarithmic dimensionless drawdown (s_{1D}/r_D^{2-n}) versus logarithmic dimensionless time(t_D/r_D^2) of, respectively, n=0.5, 1, 1.5, 2, 2.5 and 3 at an observation well in Aquifer 1 for case 2. In almost all of flow dimensions, similar to Fig. 3, one can only distinguish two parts of the curves because of long period of transition zone. The first part

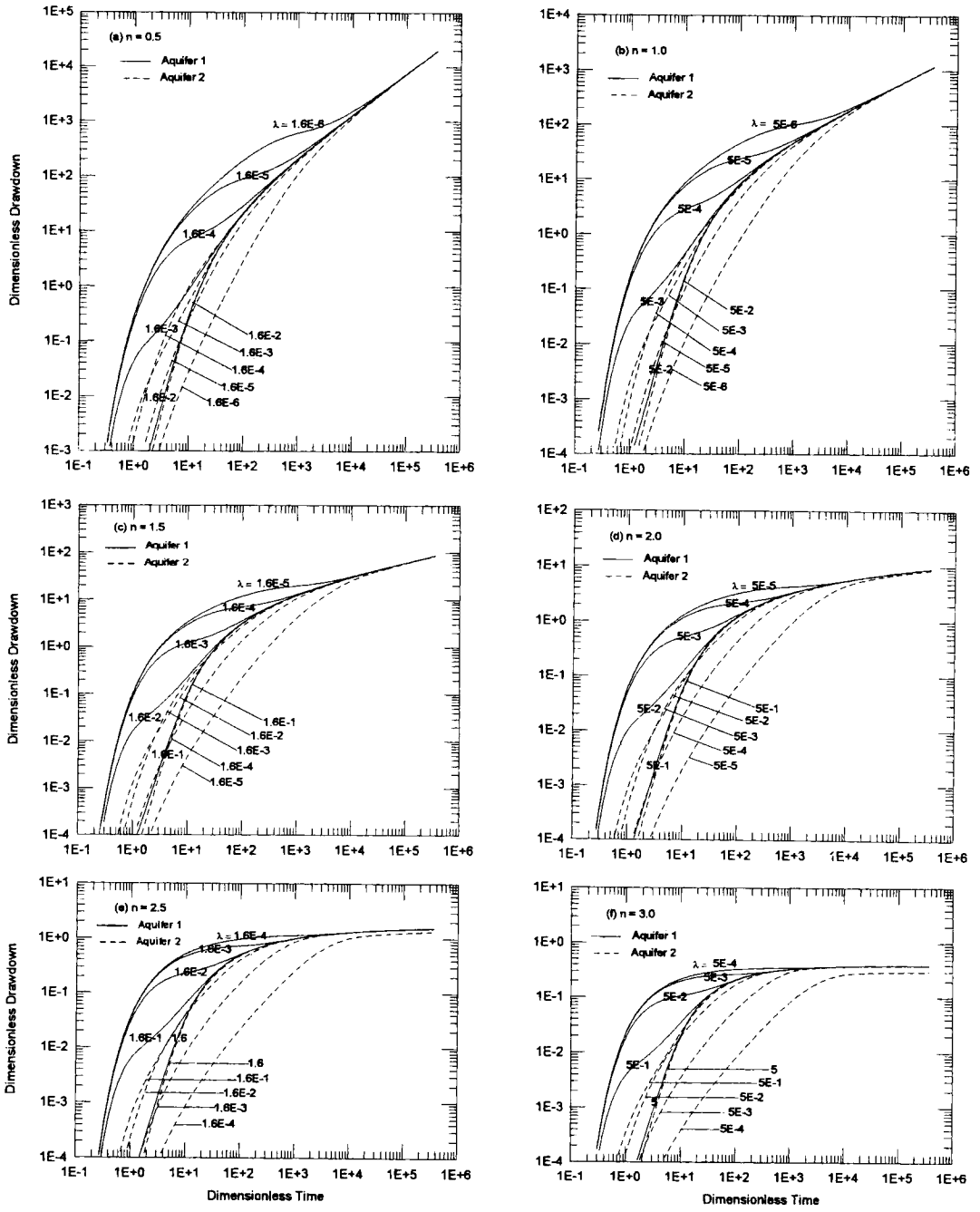

Fig. 2. Dimensionless drawdown curves at the observation wells in Aquifer 1 and Aquifer 2 with different values of λ and various flow dimensions (κ=0.99 and ω=0.091).

of the curves shows the influence of flow in Aquifer 1. The second part (the transition zone) shows important contribution from Aquifer 2 with stabilization. The smaller the value of λ, the smaller the drawdown, at early time, but the smaller the value of λ, the larger the drawdown, at late time. Broken lines of Fig. 4 (a) to (f) show logarithmic dimensionless drawdown (s_{2D}/r_D^{2-n}) versus logarithmic dimensionless time(t_D/r_D^2) of, respectively, n=0.5, 1, 1.5, 2, 2.5 and 3 at an observation well in Aquifer 2 for case 2, and are exactly the

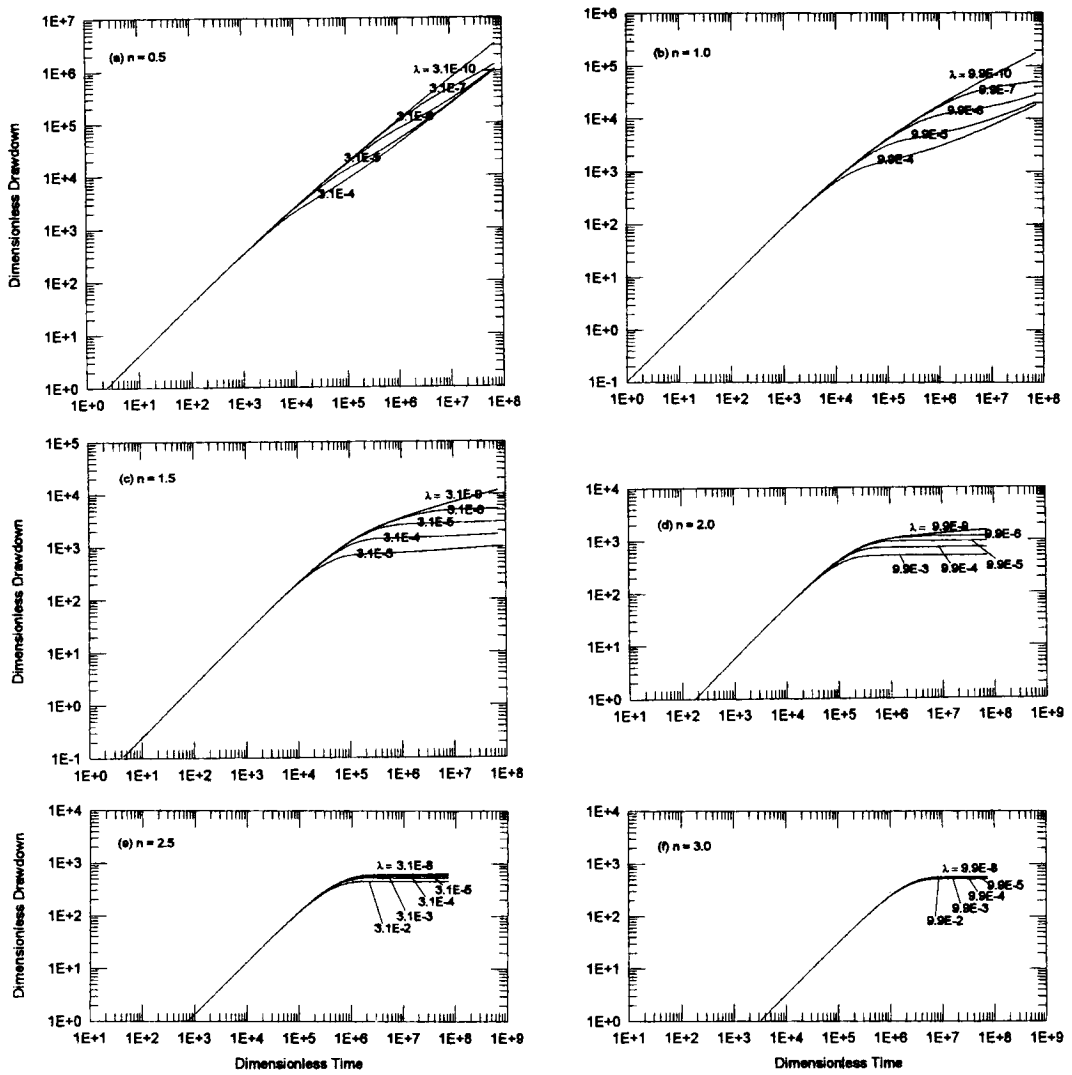

Fig. 3. Dimensionless drawdown curves at the production well in Aquifer 1 with different values of λ and various flow dimensions (W_S=0.03, S_F=0, κ=9.9E-3 and ω=0.91).

same those of Fig. 2. The larger the dimension of flow and the smaller the value of λ, the larger the differrence between the drawdown in Aquifer 1 and Aquifer 2 at late time.

CONCLUSION

A dual-permeability model of fluid flow in two superposed fractured aquifers (Aquifer 1 and Aquifer 2) was developed. The model considers wellbore storage and skin effects at the pumped well, and can be easily utilized for the multi-well and multi-rate pumping system composed of several pumping and observation wells. The model can be used when drawdown response is much different between on the pumping well and on the observation well. The phenomenon indicates the flow system of several fracture sub-networks having distinct hydraulic properties, that is, several fractured aquifers superposed. The fractal models already proposed (Barker, 1988; Chang, Yortsos, 1988; Hamm, Bidaux, 1994a, 1994b, 1996) are not suitable to analyze such data.

Several type curves for two cases - the case 1 (K_1/S_{s1} =2 m^2s^{-1}, K_2/S_{s2}=0.002 m^2s^{-1} and S_{s2}/S_{s1}=10) and the case 2 (K_1/S_{s1}=0.002 m^2s^{-1}, K_2/S_{s2}=2 m^2s^{-1} and S_{s2}/S_{s1} =0.1) - show characteristic forms of their own.

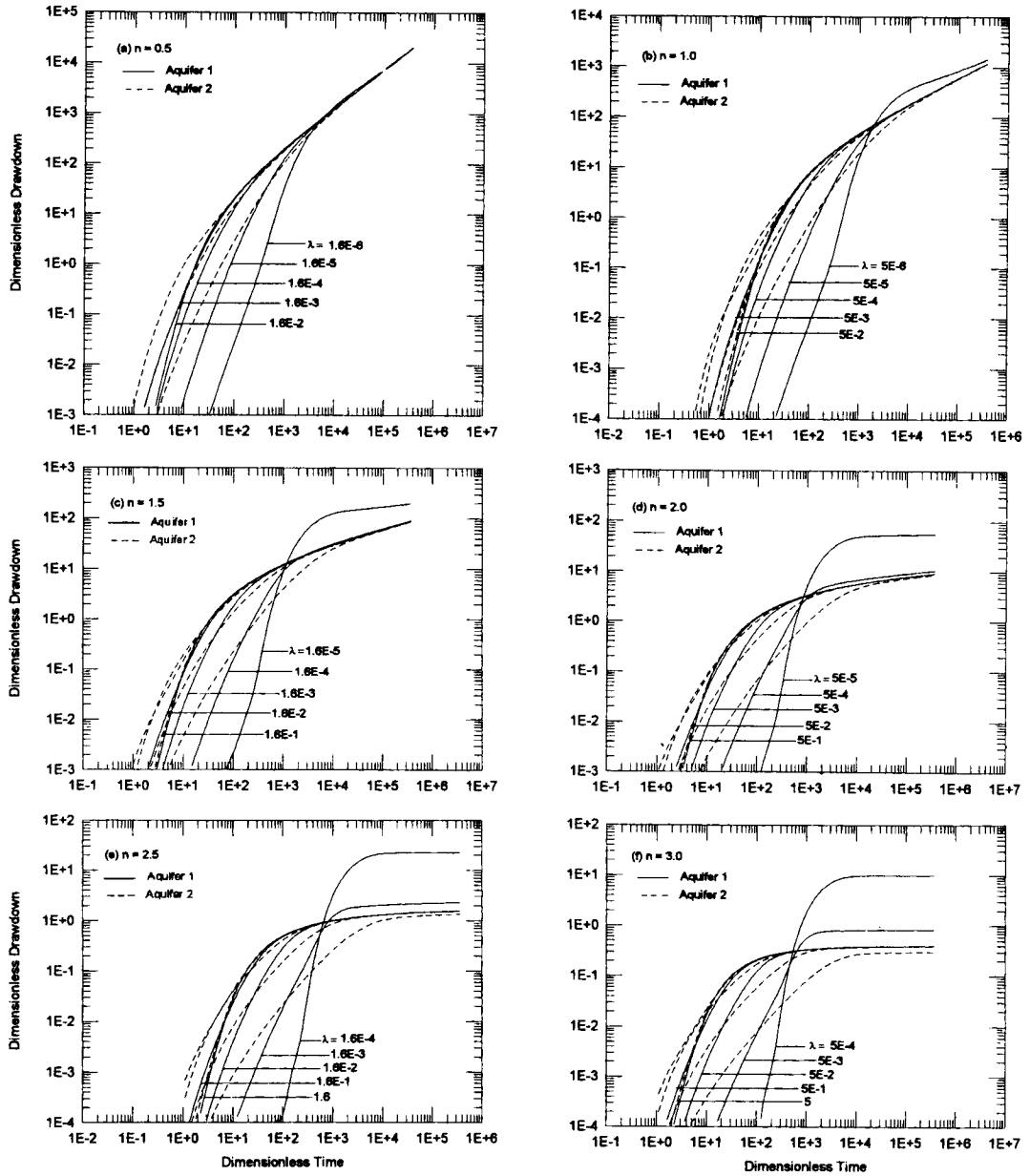

Fig. 4. Dimensiconless drawdown curves at the observation wells in Aquifer 1 and Aquifer 2 with different values of λ and various flow dimensions (κ=9.9E-3 and ω=0.91).

For the case 1, dimensionless drawdown curves of, res- pectively, n=0.5, 1, 1.5, 2, 2.5 and 3 at the pumping well (Fig. 1) and the observation well in Aquifer 1 (solid lines in Fig. 2) are similar to dual-porosity fractal model of steady-state flow (Hamm and Bidaux, 1994b). Before crossflow, flow occurs in Aquifer 1 alone without any influence in Aquifer 2. After crossflow, flow occurs in an equivalent medium that behaves like a homogenous combination of Aquifer 1 and Aquifer 2, with additional skin due to the effect of restricted entry because the source penetrates Aquifer 1 only. The straight part of the slope 1 on dimensionless curves for the pumping well (Fig. 1) represents the wellbore storage and the well loss. The smaller the value of λ, the larger the drawdown. Contrarily to the case of the observation

well in Aquifer 1, dimensionless drawdown at the observation well in Aquifer 2 (Broken lines of Fig. 2) is small when the value of λ is small.

For the case 2, The drawdown pattern of, respectively, n=0.5, 1, 1.5, 2, 2.5 and 3 at the pumping well (Fig. 3) and the observation well in Aquifer 1(solid lines in Fig. 4) are different each other. The drawdown at the pumping well is small with increasing the value of λ. On the other hand, the drawdown at the observation well in Aquifer 1 is smaller with smaller value of λ at early time, but larger at late time. The drawdown curves at the observation well in Aquifer 2 for the case 2 (Broken lines of Fig. 4) is exactly the same with those of the case 1.

ACKNOWLEDGEMENTS

The authors wish to express their gratitudes to Professor J. S. Han for careful review of the manuscript.

REFERENCES

Acuna, J.A., and Yortsos, Y.C. (1995) Application of fractal geometry to the study of networks of fractures and their pressure transient. Water Resour. Res., v. 31, p. 527-540.

Allègre, C.J., le Mouël, J.L. and Provost, A. (1982) Scaling rules in rock fractures and possible implications for earthquake prediction. Nature, v. 297, p. 47-49.

Amos, D.E. (1986) Algorithm 664: A portable package for Bessel functions of complex argument and nonnegative order. ACM Trans. Math Software, v. 12, p. 265-273.

Barenblatt, G.E., Zheltov, I.P. and Kochina, I.N. (1960) Basic concepts in the theory of seepage of homogeneous liquids in fissured rocks. Jour. Appl. Math. Mech. Engl. Transl., v. 24, p. 1286-1303.

Barker, J.A. (1988) A generalized radial flow model for hydraulic tests in fractured rock. Water Resour. Res., v. 24, p. 1796-1804.

Boulton, N.S. and Streltsova, T.D. (1977) Unsteady flow to a pumped well in a fissured water-bearing formation. Jour. Hydr., v. 35, p. 257-269.

Chang, J. and Yortsos, Y.C. (1988) Pressure-transient analysis of fractal reservoirs. SPE 18170, p. 1-14.

Cinco-Ley, H. and Samaniego-V., F. (1981) Transient pressure analysis for fractured wells. Jour. Pet. Tech., v. 33(Sept.), p. 1749-1766.

Hamm, S.-Y. and Bidaux, P. (1996), Dual-porosity fractal models for transient flow analysis in fissured rocks. Water Resour. Res., v. 32, p. 2733-2745.

Hamm, S.-Y. and Bidaux, P., (1994a) Transient flow with fractal geometry and leakage: theory and application. C. R. Acad. Sci. Paris, v. 318, Ser. 2, p. 227-233.

Hamm, S.-Y. and Bidaux, P. (1994b) Stationary dual-porosity fractal model of groundwater flow in fractured aquifers. The Jour. Eng. Geol. v. 4, p. 127-138.

Jenkins, D.N. and Prentice, J.K. (1982) Theory for aquifer test analysis in fractured rocks under linear (nonradial) flow conditions. Ground Water, v. 20, p. 12-21.

Kazemi, H. (1969) Pressure transient analysis of naturally fractured reservoirs with uniform fracture distributions. Trans. Soc. Pet. Eng. AIME, v. 246, p. 451-462.

Stehfest, H. (1970) Algorithm 368, Numerical inversion of Laplace transforms. Commun. ACM, v. 13, n. 1, p. 47-49.

Thomas, A. (1987) Structure fractale de l'architecture des champs de fractures en milieu rocheux. C. R. Acad. Sci. Paris, 304, série II, p. 181-186.

Velde, B., Dubois, J., Moore, D. and Touchard, J. (1991) Fractal patterns of fractures in granites. Earth and Planetary Science Letters, v. 104, p. 25-35.

Warren, J. E. and Root, P. J. (1963) The behavior of naturally fractured reservoirs. SPEJ, v. 3, p. 245-255.

Manuscript received 29 September 1997

균열대수층내 지하수유동에 관한 이중투수율 프락탈모델

Pascal Bidaux · 함세영

요 약 : 균열암반 이중대수층 (1대수층과 2대수층)내 지하수흐름을 모식화한 프락탈모델이 개발되었다. 이때 양수정내 지하수유입은 1대수층에서만 유래한다. 본 모델은 우물저장과 우물손실을 고려할 수 있어서 양수초기의 지하수위 변화를 정확하게 파악할 수 있는 잇점이 있다. 여러 가지 유동차원에 대해서, 1대수층의 수리전도도가 2대수층보다 더 크고, 비저유율이 2대수층보다 더 낮은 경우 (case 1)와 1대수층의 수리전도도가 2대수층보다 더 작고, 비저유율이 2대수층보다 더 큰 경우 (case 1)에 대해서 표준곡선을 작성하였으며, 이들 곡선의 특성을 분석하였다. 본 모델은 양수정과 관측정의 수위하강이 서로 다른 거동을 보여주는 양수시험자료를 해석하는데 유용하게 쓰일 수 있을 것이다.